Submitted to
Physical Review

J. Radin

UCRL-20121
Preprint

c.2

RECEIVED
LAWRENCE
RADIATION LABORATORY

MAY 14 1971

LIBRARY AND
DOCUMENTS SECTION

TWO-WEEK LOAN COPY

This is a Library Circulating Copy which may be borrowed for two weeks. For a personal retention copy, call Tech. Info. Division, Ext. 5545

α-SPALLATION CROSS SECTIONS AT 920 MeV (230 MeV/N) IN ^{27}Al, ^{16}O, ^{12}C AND ^{9}Be, AND APPLICATION TO COSMIC RAY TRANSPORT

Jonathan R. Radin, Serge A. Korff,
Alan R. Smith and Nickey Little

March 1971

Contract No. W-7405-eng-48

c.2

DISCLAIMER

This document was prepared as an account of work sponsored by the United States Government. While this document is believed to contain correct information, neither the United States Government nor any agency thereof, nor the Regents of the University of California, nor any of their employees, makes any warranty, express or implied, or assumes any legal responsibility for the accuracy, completeness, or usefulness of any information, apparatus, product, or process disclosed, or represents that its use would not infringe privately owned rights. Reference herein to any specific commercial product, process, or service by its trade name, trademark, manufacturer, or otherwise, does not necessarily constitute or imply its endorsement, recommendation, or favoring by the United States Government or any agency thereof, or the Regents of the University of California. The views and opinions of authors expressed herein do not necessarily state or reflect those of the United States Government or any agency thereof or the Regents of the University of California.

α-SPALLATION CROSS SECTIONS AT 920 MeV (230 MeV/N) IN ^{27}Al, ^{16}O, ^{12}C AND ^{9}Be, AND APPLICATION TO COSMIC RAY TRANSPORT*

Jonathan R. Radin† and Serge A. Korff
New York University
Bronx, New York 10453

and

Alan R. Smith and Nickey Little
Lawrence Radiation Laboratory
University of California
Berkeley, California 94720

March 1971

ABSTRACT

Thin-sandwich targets consisting of a monitor(s) (^{12}C and/or ^{27}Al) and primary (^{9}Be, ^{12}C, ^{16}O, and/or ^{27}Al) targets were exposed in the external 920-MeV α-particle beam at the 184-in cyclotron at Lawrence Radiation Laboratory. Cross sections for the production of ^{18}F in ^{27}Al; ^{15}O, ^{13}N, ^{11}C, and ^{7}Be in ^{16}O; ^{7}Be in ^{12}C; and ^{7}Be in ^{9}Be were measured. The results were generalized to cover all of the α-spallation cross sections in the L($3 \leq Z \leq 5$) and M($6 \leq Z \leq 8$) groups, and were applied to an analysis of the effect of the He/H+He ratio of the interstellar gas on the cosmic ray transport phenomena.

* Supported in part by the National Aeronautics and Space Administration under grant numbers NGL-33-016-067 and NAS1-5209, and by the U.S. Atomic Energy Commission.

† Present address: Tel-Aviv University, Department of Physics and Astronomy, Ramat-Aviv, Israel.

INTRODUCTION

Basic to the understanding of cosmic ray propagation is a knowledge of the nuclear spallation cross sections for reactions between cosmic rays and the interstellar gas (≈ 90% H and ≈ 10 % He).[1] Work has been directed towards the p-spallation cross sections[2] and recently towards the α-spallation cross sections.[3,4] In this paper we use the symbols (1) Σ_p^α for the generic term for the ratio of the α-particle cross section to the p cross section; (2) $\Sigma_p^\alpha(A, B)$ defined as $\sigma[A(\alpha, x)B]/\sigma[A(\beta, x)B]$, where A and B are initial and final nuclei; and (3) the function $\Sigma_p^\alpha(\Delta A)$, where ΔA is the net nucleon difference between the initial and final target states.

We report here first, on measurement of α-spallation cross sections for production of ^{7}Be in ^{12}C; of ^{7}Be, ^{11}C, ^{13}N, and ^{15}O in ^{16}O; of ^{7}Be in ^{9}Be; and of ^{18}F in ^{27}Al. Second, with the assumption of (1) a linear dependence of $\Sigma_p^\alpha(\Delta A)$ on ΔA, with E_p equal to the total α-particle kinetic energy ($E_{\alpha T}$), and (2) cosmic rays consisting of L($3 \leq Z \leq 5$) and M($6 \leq Z \leq 8$) nuclei exclusively, we examined the sensitivity of (1) the mass of interstellar gas traversed to produce an L/M ratio of 0.25,[5] and (2) the elemental abundances at L/M = 0.25, as a function of the He/H+He ratio of the interstellar gas. The transport model chosen was the one-dimensional slab approximation wherein all species traverse an equal amount of matter.

EXPERIMENTAL PROCEDURES

Targets consisting of 3.81-cm-diam thin sandwiches (Fig. 1) were exposed to the external 920-MeV (230-MeV/N) α-particle beam in the medical cave of the 184-in. cyclotron at Lawrence Radiation

Laboratory (LRL). The beam was focused to a diameter of ≈ 2.5 cm on which targets were centered. The neutron and deuteron contaminations of the beam had been studied previously and were negligible.[3] The targets were counted in the low-background cave of the Health Physics Group at LRL. The ^{16}O target was BeO and, as the Be (100% ^{9}Be) present contributed to the ^{7}Be production, $\sigma[^9Be(\alpha, x)^7Be]$ was determined with Be targets. In Table I, the pertinent information of the isotopes examined is tabulated.[6]

TARGETS

All targets (Fig. 1) are sandwiches, 3.81 cm diam, consisting of two or three subtargets [main and monitor(s)]. Each subtarget consists of guard foils or disks and the central counted disk. The constituents are:

^{12}C--polystyrene, $(CH)_n$, disks 0.16 cm (0.17 g/cm^2) thick, with 0.008-cm polyethylene guard foils. The carbon cross sections are based on the total carbon (^{12}C + ^{13}C) content.

BeO--ceramic disks, 0.075 cm (0.26 g/cm^2) and 0.32 cm (0.95 g/cm^2) thick, and 99.5% pure. The front and rear guard disks are 0.075-cm and 0.32-cm BeO disks, respectively. The contamination was determined by spectrometric analysis to be $(1.0^{+1.0}_{-0.5})$% Mg plus trace quantities of other elements. The oxygen was taken to be 100% ^{16}O.

Be--a vacuum-deposited Be disk (impurity 60 ppm), 0.075 cm (0.13 g/cm^2) thick. The front and rear guard disks are 0.02-cm and 0.32-cm Be. No radiation other than ^{7}Be was observed.

Al--99.99% Al foils of thickness 0.008 cm (0.023 g/cm^2) for monitoring and 0.013 cm (0.035 g/cm^2) for $\sigma[^{27}Al(\alpha,x)^{18}F]$ determinations. The guard foils are 0.004 cm thick.

BEAM MONITORS

The beam monitors for all cross section determinations were radioisotopes produced in the target disks. For short (not ^{7}Be) half-lives, the $^{12}C(\alpha,x)^{11}C$ reaction with a cross section of 49.4 ± 1.8 mb was used.[3] For ^{7}Be production runs, exposure times of 2-10 min required a longer half-life monitor and the $^{27}Al(\alpha,x)^{18}F$ reaction was used. This cross section was separately determined relative to the $^{12}C(\alpha,x)^{11}C$ reaction, yielding $\sigma[^{27}Al(\alpha,x)^{18}F]$ = 12.6 ± 0.5 mb. In addition, as there were many $^{12}C(\alpha,x)^7Be$ runs, all in good agreement; the $^{12}C(\alpha,x)^7Be$ reaction in the polystyrene, with a cross section of 20.2 ± 1.1 mb, was used as an additional monitor for the ^{7}Be production runs in BeO and Be.

COUNTING APPARATUS

The detection system consisted of a 20.4-cm diam × 10.2-cm thick NaI(Tl) crystal, optically coupled with Dow-Corning DC 200 silicone grease to a 5-in. diam EMI 9530-Q photomultiplier (face plate and part of the envelope are fused quartz). The system is housed inside 10.2 cm of low activity lead bricks. A more complete description is found in the reference.[7] After exposure, the β^+-decaying targets were placed between Cu plates sufficiently thick to stop the β^+; the γ-decaying targets were placed directly on the cover plate of the NaI crystal. The output of the photomultiplier was preamplified,

double-delay-line shaped, and then pulse-height analyzed by a gain-stabilized 1600-channel Victoreen (SCIPP 1600) analyzer. For β^+ accumulation, the gain was stabilized on the 511-keV peak and for ^{7}Be on the 478-keV peak. In all cases the counting interval was 380-610 keV. The peaks were accumulated in the live-time mode, wherein the counting time is extended to compensate for the signal-analysis time, during which no new signal is accepted. The dead time was extensively analyzed (see Appendix). To minimize dead-time corrections, no counts were used in the fittings when count rates were $>150\times10^3$/min, except for one $^{16}O \rightarrow {}^{15}O$ run. The largest corrections were for $^{16}O \rightarrow {}^{15}O$, which resulted in 3% changes in the initial quantities of ^{15}O produced by the fitting algorithm.

RUNS AND FITTINGS

There were two runs to determine the $\sigma[^{27}Al(\alpha,x)^{18}F]/\sigma[^{12}C(\alpha,x)^{11}C]$ ratio and the resultant cross section. Initial counts were recorded in 1-min intervals, and the target was counted for several days. The β^+ peak was least-squares fitted to half-lives of 2.05 min (^{15}O), 9.96 min (^{13}N), 20.35 min (^{11}C), 109.7 min (^{18}F), and 894 min (^{24}Na); the background was both free and fixed (a 10-min ^{27}Mg component was observed but not analyzed). The fitted ^{18}F was found insensitive (< 1% initial quantity changes) to variations at the ends of the fitting routine: (1) at the short half-life end by varying the time between the end of exposure and the start of the fitting routine, and by inclusion of a 1 min half-life in the fit; and (2) at the long half-life end by varying the time between the end of exposure and the end of the fitting routine, and by letting background be both

fitted and fixed (fitted and observed background agreed to within 5%). The initial quantity of ^{18}F was determined, relative to the ^{11}C in the monitor, to within 2%.

There were six runs to determine the two ratios of $\sigma[^{12}C(\alpha,x)^{7}Be]$ to σ(monitor reaction) and the subsequent cross section. One run produced a large χ^2 in the fit and was not included in the final averaging. There were two runs to determine the three ratios of $\sigma[^{9}Be(\alpha,x)^{7}Be]$ to σ(monitor reaction). The Be target was reused, and the residual ^{7}Be in the second exposure was carefully determined) to be $(32.5 \pm 0.5)\%$ of the ^{7}Be produced in the second exposure. Both runs agreed to within 1%.

There were three runs to determine the ratio of cross section to monitor-reaction cross section for ^{15}O, ^{13}N, and ^{11}C production in ^{16}O, and two runs to determine the three ratios of $\sigma[BeO(\alpha,x)^{7}Be]$ to σ(monitor reaction). The third run for ^{15}O production, reusing the previous target, inexplicably gave a small cross section, much in disagreement with the other two runs, and was not included in the final averages. For the short-half-life runs the counts were accumulated at 1-min intervals and least-squares fitted to 2.05, 9.96, and 20.35-min half-lives. The variations in the fitting routine discussed for the $^{27}Al(\alpha,x)^{18}F$ runs were repeated here, except for excluding a fit to a 1-min half-life component. This procedure resulted in uncertainties in the quantities produced in the three exposures of 2% for ^{15}O and ^{11}C, and 3%, 6%, and 6% for ^{13}N. The ratios of $\sigma[^{16}O(\alpha,x)^{7}Be]$ to the three monitor-reaction cross sections were determined by subtracting the ratio of $\sigma[^{9}Be(\alpha,x)^{7}Be]$ to σ(monitor reaction) from the ratios of $\sigma[BeO(\alpha,x)^{7}Be$ to σ(monitor reaction). In

Tables II and III are tabulated the quantities of interest regarding the ratios of cross section to σ(monitor reaction) and the resultant cross sections (Fig. 2).

UNCERTAINTIES

The efficiency of the NaI(Tl) system for β^+ emission, not of primary concern, was determined relative to the absolute C^{11} efficiency detector,[3] and was $(52.2 \pm 1)\%$. The efficiency of the NaI(Tl) for the 478-keV γ of ^{7}Be was taken to be the same as for the 511-keV annihilation γ within a systematic error of 1%. The ^{7}Be efficiency differed from the β^+ efficiency in three ways (which were corrected). First, the spectrum of the β^+ showed, in addition to the primary peak at 511 keV, a second peak at 710 keV which was the sum peak of one annihilation γ plus the backscattered second γ. The energy sum of a 511-keV and[2] 180°-backscattered 511-keV γ was 767 keV, consistent with the peak location. The area under the sum peak was found to be $(5.7 \pm 0.2)\%$ of the area of the main peak. Second, the Cu plates around the β^+ emitters attenuated the 511-keV γ. Third, the Cu plates separated the β^+ emitters from the NaI by 0.16 cm more than the ^{7}Be counted targets. To correct for the last two effects, a ^{7}Be active target was counted inside the Cu plates in the β^+ counting configuration and on the NaI in the ^{7}Be configuration, yielding a correction of $(14.5 \pm 2)\%$ to the ^{7}Be efficiency.

The self-absorption of the targets was theoretically corrected. The largest correction was $(2 \pm 1)\%$ for the 10.8-g BeO. The correction to an infinitely thin target was made with the assumption that the correction for all targets and products was the same and equal to the

$^{12}C(\alpha, x)^{11}C$ depth effect in polystyrene[3] of $(0.26 \pm 0.10)\%/100$ mg cm^{-2}. The 0.16-cm polystyrene disks were assumed to lose $(0.4 \pm 0.4)\%$ of the ^{11}C by diffusion.[8]

The random errors are

1. initial quantity of the isotopes produced,
2. time at end of exposure, ±1 sec,
3. background in the interval examined, 81 ± 1 counts/min,
4. target alignment, ±1%,
5. diffusion loss of ^{11}C in the polystyrene, ±0.4%,
6. uncertainty in the monitor cross sections.

The systematic errors are

1. relative efficiency of the NaI(Tl) crystal for 478-keV γ's ± 1%,
2. annihilation-γ sum peak, ±0.2%,
3. annihilation-γ absorption in the target holder, ± 2%,
4. contamination in the BeO, ± 1%.

In Table III the α-particle cross sections, the p cross sections at $E_p = E_\alpha$ and $E_p = E_{\alpha T}$, and Σ_p^α at the two proton energies are tabulated. The random and systematic errors, where apropos, were separately rms-combined and then added to give the error estimates in Tables II and III (Fig. 2).

The $^9Be(p, x)^7Be$ cross sections at the two proton energies were derived from the excitation function (Fig. 3), which was determined from the following adjusted cross sections:

Energy (MeV)	σ (mb)	σ Adjusted (mb)	Author	Ref
156	8.8 ± 0.5	8.8 ± 0.5	Valentin et al.	9
352	12.0 ± 0.5	14.8 ± 0.6	Parikh	10
5700	15	12.5 ± 1	Benioff	11

The adjusting factor for Parikh is the ratio of $\sigma[^{12}C(p, x)^7Be]$, measured by him (8.3 ± 0.3 mb), to that of Cumming (10.2 ± 1 mb).[12] The adjusting factor for Benioff is the ratio of $\sigma[^{27}Al(p, x)^{18}F]$, used as a monitor by him (7.68 mb), to that for Cumming (6.5 ± 0.4 mb).[12]

The $^{16}O(p, x)^7Be$ excitation function, included in Fig. 3 for convenience, is derived from the compilation by Silberberg,[13] wherein $\sigma[^{16}O(p, x)^7Be]$ over the range 200 MeV $\leq E_p \leq$ 2 GeV is fitted to

$$\sigma = 3.25 \log_{10}[E_p(\text{MeV})] - 1.75 \pm 1.5 \text{ mb},$$

and over the range $E_p > 6$ GeV to $\sigma = 10 \pm 1.5$ mb (Fig. 3).

COSMIC RAY PROPAGATION

The interactions with the interstellar gas were parameterized by (1) the mean free path for absorption (Λ_{abs}), (2) the fragmentation probability of the absorbed i-nucleus into the j-nucleus (P_{ij}), and (3) the ionization-energy loss of the isotopes. With the assumption that cosmic rays consist only of L and M isotopes, we investigated the sensitivity of the L/M ratio and the elemental abundances to the He/H+He ratio of the interstellar gas. In addition, we examined the sensitivity of these two quantities with the separate

variations of the three interaction parameters (Λ_{abs}, P_{ij}, and dE/dx), to discern which are most crucial, and consequently, which most need improved experimental accuracy. The one-dimensional transport equation used, iterated in steps of $\Delta x = 0.1$ g/cm^2, is

$$N_i(E_i', x+\Delta x)dE_i' = N_i(E_i, x)\, e^{-\Delta x/\Lambda_i} dE_i + \sum_{j>i} N_j(E_j', x+\Delta x) P_{ji}(1 - e^{-\Delta x/\Lambda_j}) dE_j', \quad (1)$$

where the following definitions and formulas are used:

all energies are in kinetic energy/nucleon;

$N_i(E_i, x)dE_i$ is the flux of isotope$_i$ from E_i to $E_i + dE_i$ after traversal of x g/cm^2;

F_i = fraction of atoms of interstellar gas of element$_i$ (H and He), e.g., F_{He} = He/H+He;

m_i = mass of element$_i$ in grams;

$\sigma^k_{i,re}$ = reaction cross section for isotope$_i$ in target$_k$ ($k = p, \alpha$);

$\sigma^k_{i,j}$ = cross section for production of i from $j + k \rightarrow i +$, ($k = p, \alpha$);

Λ_j = mean free path for interaction in g/cm^2 = $\sum_{i=p}^{\alpha} F_i m_i / \sum_{i=p}^{\alpha} F_i \sigma^i_{j,re}$;

P_{ij} = fragmentation probability = $\sum_{k=p}^{\alpha} F_k \sigma^k_{i,j} / \sum_{k=p}^{\alpha} F_k \sigma^k_{j,re}$.

Eleven isotopes are transported--^{6}Li, ^{7}Be, ^{7}Li, ^{9}Be, ^{10}B, ^{11}B, ^{12}C, ^{13}C, ^{14}N, ^{15}N, and ^{16}O. ^{7}Be is considered stable. For simplicity ^{10}Be, whose p-spallation production cross section[14] in ^{16}O is < 0.1 that of ^{7}Be, is neglected (although results by Fontes et al.[4] for p + ^{12}C spallation at 600 MeV show the ^{10}Be/^{7}Be ratio to be

0.25 ± 0.03, indicating that the ^{10}Be is nonnegligible). The calculation is performed at 2 GeV/N. The source spectrum is taken to be rigidity dependent with spectral index -2.2.[15] This number is less than the usual rigidity-spectral index of -2.5; however, at 3 GeV/N the calculation is insensitive to this parameter as all isotopes are minimum ionizing. The source distribution is taken to be 0.0 except for

$$^{12}C:\ ^{14}N:\ ^{16}O = 1.00:0.11:1.06 \text{ (Ref. 16).}$$

The proton cross sections are taken from Beck and Yiou[17] and Yiou et al.[14] The cross sections used here differ from those of Beck and Yiou only for the ^{6}Li, ^{7}Li, ^{9}Be, and ^{10}B production cross sections in ^{16}O, taken here as 13.5, 13.5, 3.3, and 14 mb respectively. The α-particle cross sections are treated as follows.

It has been shown[3] that Σ_p^α (^{12}C, ^{11}C) with $E_p = E_{\alpha T}$, for 380 MeV $\leq E_{\alpha T} \leq$ 920 MeV, is constant (= 1.7). Also, $\sigma[^{12}C(p,pn)^{11}C]$ is constant within experimental errors (± 5%) from 1 to 30 GeV.[10] Assuming that Σ_p^α (^{12}C, ^{11}C) remains constant, at least in the range 1 GeV $\leq E_p (= E_{\alpha T}) \leq$ 10 GeV, then $\sigma[^{12}C(\alpha,x)^{11}C]$ is also constant in that range (250 MeV/N $\leq E_\alpha \leq$ 2.5 GeV/N). It is probably safe to extend this argument to all "simple" reactions (1-2 nucleons removed). In addition, for the purpose of the calculation at 2 GeV/N, we make the ensatz that Σ_p^α for each initial and final nuclide of the L and M elements, with $E_p = E_{\alpha T}$, is a constant function of $E_{\alpha T}$ in the range 1 GeV $\leq E_{\alpha T} \leq$ 10 GeV. Again, as the proton cross sections vary little from 1 to 10 GeV, we deduce that the α-particle cross sections measured at 230 MeV/N (920 MeV) will be constant to 2.5 GeV/N (10 GeV) within experimental errors. At $E_p = E_{\alpha T}$ = 1 GeV, by use of

the data tabulated in Table III for ^{12}C and ^{16}O spallation, $\Sigma_p^\alpha(\Delta A)$ was least-squares fitted to $\Sigma_p^\alpha(\Delta A) = a + b\Delta A$. The fit is sensitive to $\Sigma_p^\alpha(^{16}O, {}^7Be)$. The values of $\sigma[^{16}O(p,x)^7Be]$ from Table III, at 1 GeV (or 2 GeV), of 8.0 ± 1.5 mb (or 9.0 ± 1.5 mb), yield $\Sigma_p^\alpha(^{16}O, {}^7Be) = 2.34 \pm 0.5$ (or 2.07 ± 0.4), and the coefficients in the $\Sigma_p^\alpha(\Delta A)$ linear fit of $a = 1.64 \pm 0.07$ (or 1.67 ± 0.07) and $b = 0.065 \pm 0.03$ (or 0.050 ± 0.02), and χ^2 per degree of freedom, in both cases, of 0.4 (Fig. 3). We conservatively chose the latter set of parameters for $\Sigma_p^\alpha(\Delta A)$ to scale all the α-particle cross sections onto the p cross sections at 2 GeV.

The spallation process in the Serber two-step model[18] is considered as a knock-on plus evaporation. Munir has shown[19] that the L nuclei produced in p + M nuclei reactions, at $E_p = 1$ GeV, can be interpreted as evaporation residues with, on the average, small (≈ 12 MeV) energy transfers. For all spallation reactions, we have taken the initial and final kinetic energy per nucleon to be equal.

Values for $\Lambda_{^4He\ abs}$ had to be derived from models as, to the authors' knowledge, there have been no experiments measuring inelastic or absorption cross sections of ^4He nuclei of known energy, > 100 MeV/N, in single-element targets. We compared (a) two nucleus-nucleus reaction cross-section models, (b) the independent-particle optical-potential model of Alexander and Yekutieli[20] (with a free nucleon-nucleon cross section of 40 mb), and (c) three versions of the overlap model

$$\sigma_{i,re}^{\alpha} = \pi(r_0 A_\alpha^{1/3} + r_0 A_i^{1/3} - \Delta r)^2, \qquad (2)$$

first proposed by Bradt and Peters ($r_0 = 1.45$ F, $\Delta r = 1.70$ F),[21] and modified by Daniel and Durgaprasad ($r_0 = 1.17$ F, $\Delta r = 0$),[22] and by

Cleghorn ($r_0 = 1.20$ F, $\Delta r = 0.50$ F).[23] Tests of the models come from the many experiments measuring $\Lambda_{He\ abs}$ of cosmic ray α particles in emulsion (e.g., compilation by Waddington),[24] and the attenuation mean free path (Λ_{atn}) of cosmic ray α-particles in the atmosphere. From the measurements of the latter quantity by Webber and McDonald,[25] Davis et al.,[26] McDonald,[27] and Webber and Ormes,[15] of 43 ± 8, 35 ± 7, 45 ± 7, and 52 ± 4 g/cm^2 respectively, the value of 44 g/cm^2 was chosen. For α-particle interactions in emulsion we used $\sigma_{\alpha,re}^p$ of 125 mb.[28] In identifying $\Lambda_{^4He\ abs}$ in L and M elements from emulsion experiments, there is uncertainty in that $\approx 60\%$ of the reactions occur with Ag and Br and $\approx 30\%$ with C, N, and O. In air there is uncertainty arising from the fragmentation of the heavier-than-He cosmic rays, and from the $^4He \rightarrow {}^3He$ stripping reactions. In air, we have estimated the errors as a result of equating, $\Lambda_{^4He\ abs} = \Lambda_{He\ atn}$ from the two above processes, to be $\leq (9-14)\%$ and $\leq 30\%$ respectively (see Appendix). Consequently, for air, we have taken $\Lambda_{^4He\ abs} = \Lambda_{He\ atn} = 44$ g/cm^2, but not seriously; and for emulsion we have taken $\Lambda_{^4He\ abs} = 77$ g/cm^2. In Table IV, the four models are intercompared. The overlap model of Cleghorn was chosen, but tests of all the models showed that the choice was inconsequential; it yielded less than 0.5% differences in the quantity of interstellar gas traversed, with He/H + He = 0.2, to produce L/M = 0.25.

In Table V are tabulated the results of the calculation. Columns 1-3 give the value of He/H + He used for the individual parameters Λ_i, P_{ij}, and dE/dx; columns 4-7 are the amounts of matter traversed to reach L/M = 0.25, in g/cm^2 and atoms/(cm^2 N_0). Columns 8-12 are the elemental ratios with respect to carbon. Row 1 is

the observed elemental ratios from the experiments of von Rosenvinge et al.[5] and Lezniak et al.,[29] and from the compilations of Shapiro et al.[16,30] Row 2 gives the calculated elemental ratios for He/H+He = 0.0. For the remaining rows, the elemental ratios are in percent differences from the calculated ratios for He/H+He = 0.0. The mass of interstellar gas traversed to reach L/M = 0.25, and the elemental ratios obtained by varying Λ_i, P_{ij}, and dE/dx one at a time, for He/H+He = 0.1, were derived from their values for He/H+He = 0.2 by multiplying by the factor 0.541 ± 0.02 (see following).

The fractional changes in the mass of interstellar gas traversed to reach L/M = 0.25 and the elemental ratios for R ≡ He/H+He = 0.1 and 0.2, relative to 0.0, were fitted to $F(R) = gRe^{-hR}$. Normalizing on F(0.1) = 0.1, and allowing for a multiplicative constant (g) for each of the fitted quantities (Row 3, He/H+He = 0.1 for Λ_i, P_{ij}, and dE/dx), yields h = 0.78 ± 0.3, Table V and F(0.1)/F(0.2) = 0.541 ± 0.02. The fractional increase in the mass traversed to reach L/M = 0.25 over the range 0 ≤ (He/H+He) ≤ 1.0, relative to He/H+He = 0.0, fitted to the same functional form (unnormalized), produced g = 1.94 and h = 0.560 (Fig. 6). Differences between the fitted [F(R)] and calculated values were < 3%.

The interpretation of the separate and combined variations of Λ_i, P_{ij}, and dE/dx is simpler when the quantity [(% elemental abundance change)-⟨% elemental abundance change in L or M⟩] is examined for He/H+He = 0.1 relative to 0.0, which quantity is decoupled from the carbon variations found in the elemental ratios. We can treat the L and M groups separately, as the L/M ratio is always a fixed parameter. We define

$$Y \equiv \frac{d}{dA_i}\left(\frac{D(N_i)}{N_i} - \left\langle\frac{D(N_i)}{N_i}\right\rangle \text{ L or M}\right), \tag{3}$$

where

$$D(N_i) = N_i(\text{He/H+He}) - N_i(0,0). \tag{4}$$

Within the L and M groups, we observe in Fig. 6 that the effect on Y of varying the individual parameters Λ_i, P_{ij}, and dE/dx with He/H+He = 0.1, is

Y > 0	for Λ_i variation,
Y < 0	for P_{ij} variation,
Y negligible	for dE/dx variation.

This can be explained with the transport equation. If ionization energy loss is neglected, and with $\Delta x << \Lambda_j < \Lambda_i$, Eq. (1) becomes

$$\Delta N_i = N_i(x+\Delta x) - N_i(x) = -N_i(x)\frac{\Delta x}{\Lambda_i} + \sum_{j>i} N_j(x+\Delta x)P_{ji}\frac{\Delta x}{\Lambda_j}. \tag{5}$$

The sensitivity of N_i to the He/H+He of the interstellar gas is approximately the sensitivity of ΔN_i to the He/H+He, where ΔN_i, as above, corresponds to a single increment, Δx of x. Operating on ΔN with D, as defined in Eq. (4), we have

$$D(\Delta N_i) = N_i(x)D\left(\frac{-\Delta x}{\Lambda_i}\right) + \sum_{j>i} N_j(x+\Delta x)D\left(P_{ji}\frac{\Delta x}{\Lambda_j}\right), \tag{6}$$

and

$$\frac{d}{dA_i}D(\Delta N_i) \cong Y. \tag{7}$$

For any argument $G(\Lambda_i, P_{ji})$ of D in Eq. (6),

$$D(G) \equiv \frac{\partial G}{\partial \Lambda_i}D(\Lambda_i) + \frac{\Lambda G}{\Lambda P_{ji}}D(P_{ji}). \tag{8}$$

Writing $\Lambda_i \propto \frac{1}{\sigma_{i,re}} \cong \frac{1}{(C+A_i^{1/3})^2}$, where $c = c(He/H+He)$ (9)

$c \approx 0$ in hydrogen

$c > 0$ in helium

and considering the case when only Λ_i is dependent on the He/H+He, one has

$$D(A_i) \cong \frac{\partial \Lambda_i}{\partial c} c, \tag{10}$$

and from partial enactment of the chain rule of Eq. (8),

$$D(P_{ji} \frac{\Delta x}{\Lambda_j} \cong P_{ji} D(\frac{\Delta x}{\Lambda_j}). \tag{11}$$

Substituting Eq. (11) into the last term of Eq. (6), becomes

$$D(\Delta N_i) = N_i(x) D(\frac{-\Delta x}{\Lambda_i}) + \sum_{j>i} N_j(x+\Delta x) P_{ji} D(\frac{\Delta x}{\Lambda_j}). \tag{12}$$

The second term is much smaller than the first term, as P_{ji} are $<<1$, and is dropped. Substituting Eq. (12), less the second term, into Eq. (7), and applying Eq. (8) and Eq. (10), gives

$$Y \approx N_i(x) \frac{d}{dA_i} D(\frac{-\Delta x}{\Lambda_i}) \cong N_i(x)\, c\, \Delta x \left(\frac{-2}{d\Lambda_i} \frac{d\Lambda_i}{dA_i} + \frac{1}{\Lambda_i^2} \frac{d^2\Lambda_i}{dc\,dA_i}\right)\Big|_{c=0} > 0, \tag{13}$$

as observed in Fig. 6 for $\Lambda_i \cong \Lambda_i(He/H+He)$.

Considering the case when only P_{ji} is dependent on the He/H+He and taking for simplicity the case of He/H+He = 1.0, then

$$D(P_{ji}) = \frac{\sigma_{i,j}^{\alpha}}{\sigma_{j,re}^{\alpha}} - \frac{\sigma_{i,j}^{p}}{\sigma_{j,re}^{p}} = \frac{\Sigma_p^{\alpha}(A_j - A_i)\sigma_{i,j}^{p}}{\sigma_{j,re}^{\alpha}} - \frac{\sigma_{i,re}^{p}}{\sigma_{j,re}^{p}}$$
$$= \left[\frac{\sigma_{j,re}^{p}}{\sigma_{j,re}^{\alpha}} \sum_p^{\alpha} (A_j - A_i) - 1\right] \frac{\sigma_{i,j}^{p}}{\sigma_{j,re}^{p}}. \tag{14}$$

In Eq. (6), the first term is zero. Substituting Eq. (14) in the second term of Eq. (6), then

$$D(\Delta N_i) = \sum_{j=i} N_j(x+\Delta x) \frac{\Delta x}{\Lambda_i} \left[\frac{\sigma_{j,re}^{p}}{\sigma_{j,re}^{\alpha}} \sum_p^{\alpha} (A_j - A_i) - 1\right] \frac{\sigma_{i,j}^{p}}{\sigma_{j,re}^{p}}. \tag{15}$$

We observe in Eq. (15) that the only explicit A_i dependence is in the cross-section scaling factor whose derivative with respect to A_i is

$$\frac{d}{dA_i} \sum_p^{\alpha} (A_j - A_i) = \frac{d}{dA_i} [a + b(A_j - A_i)] = -b. \tag{16}$$

Substituting Eq. (15) and Eq. (16) into Eq. (7), we have

$$Y \cong (-b) < 0, \tag{17}$$

as observed in Fig. 6 for $P_{ji} = P_{ji}$ (He/H+He).

Until recently, the slab approximation to the transport problem, i.e., a delta-function path-length distribution, has been the accepted model. A more theoretically satisfying model, which also produces better agreement with experiments, is the exponential path-length model,[31, 32] which is similar to the product of diffusion theory with simple boundary conditions.[33, 32] The path-length model chosen is second order on the relative effects of the He/H+He ratio of the interstellar gas. Examining the fractional changes in the quantity [L/M(He/H+He = 0.2) - L/M(0.0)]/[L/M(0.0)], evaluated at x = 0.5 g/cm^2 and 5.0 g/cm^2 of interstellar gas traversed, we concluded that differences arising in all the calculated fractional changes in the quantities of Table V, between the slab and exponential path-length models, is < 5%.

CONCLUSIONS

The effect of the ≈ 10% He component in the interstellar gas does not have pronounced effects (<2%) on the cosmic ray L and M elemental abundances at 2 GeV/N. As a consequence of the nonconstant $\Sigma_p^\alpha(\Delta A)$, the P_{ij}, in general, have a greater effect on the elemental ratios than Λ_i. It is to be noted that at 230 MeV/N, $\Sigma_p^\alpha(^{16}O, ^7Be)$ is 3.2 ± 0.8 owing to the lower value of $\sigma[^{16}O(p, x)^7Be]$ ($= 5.9 \pm 1.5$ mb) at this energy. The ≈ 10% He in the interstellar gas, at this energy, is responsible for ≈ 25% of the ^{7}Be production. As this energy is near the now uncertain peak in the L/M ratio of ≈ 0.40 (200-700) MeV/N,[34] further investigation beckons. Additional data are needed for the α-spallation reactions in Fe, L, and M groups at $E_\alpha > 50$ MeV/N.

ACKNOWLEDGMENTS

We warmly thank, and acknowledge the support and continuous aid of, the Nuclear Emulsion Group at LRL, especially Harry H. Heckman, Douglass Greiner, and Peter Lindstrom. We thank Robert Kuntz of LRL at Livermore for providing the Be target. We are indebted to the 184-in. cyclotron crew headed by Jimmy Vale. We acknowledge the help of the entire Cosmic Ray Group at New York University, in particular, Rosalind B. Mendell.

APPENDIX

Dead Time There are two effective detector-system times: the Victoreen analyzer signal-analysis time (τ_{sat}) during which no new signal is accepted, and the preamplifier deat time (τ_{adt}). The analyzer was operated in the live-time mode wherein the counting time is extended to compensate for counts lost during τ_{sat}. For infinite half-lives, the compensation was assumed to be exact, i.e., [number of counts] ∝ [source activity]. But with short half-lives (half-life ≲ counting time) and high count rates [(count rate)$^{-1}$ ≲ τ_{sat}], counts are lost (the case with ^{15}O). To compensate, τ_{sat} and a functional form for the counting-time extension (F) was found. Counting a hot ^{11}C source for several half-lives, tabulating the laboratory counting time (LAB), the analyzer live time (LIV), and the count rate (n), for LIV = 1-min intervals, and writing LAB = LIV · F(n, τ_{sat}), one is led by Poisson statistics to setting $F = \exp(n\tau_{sat})$. But a better fit was found for the first-order expansion $F = 1 + n\tau_{sat}$, which says that the fractional time extension is proportional to the count rate. Here, τ_{sat} was determined by a least-squares fit of the tabulated LAB, LIV, and n to be 19 μsec. If the amount of material with mean life τ at time t is $I(t) = I_0 e^{-t/\tau}$, then the count rate at time t is $(I_0/\tau)e^{-t/\tau}$, and the average count rate in the interval $0 \leqq t \leqq$ is $(I_0/\tau)(1 - e^{-T/\tau})$. Defining the fractional counts lost in time LAB as FCL[LAB, LIV (n, τ)], then, to first-order, FCL ≃ (⟨count rate in LIV⟩ - ⟨count rate in LAB⟩)/⟨count rate in LAB⟩,

$$\mathrm{FCL} \cong \frac{[(\frac{1}{\mathrm{LIV}})(1-e^{-\mathrm{LIV}/\tau}) - (\frac{1}{\mathrm{LAB}}(1-e^{-\mathrm{LAB}/\tau})]}{(\frac{1}{\mathrm{LAB}})(1-e^{-\mathrm{LAB}/\tau})}. \quad (18)$$

For $\tau \ll$ (LAB-LIV), the expression reduces to FCL = (LAB-LIV)/2τ = $(n\tau_{sat}\,\mathrm{LIV})/2\tau$. For the case of ^{15}O with τ = 3 min, n = 200×10^3 counts/min, and LIV = 1 min, the fractional counts lost ≈ 1.5%. With N multicomponent decays, of mean life τ_i, the expression for the fractional counts lost is

$$\mathrm{FCL} \cong \sum_{i=1}^{N} \frac{\left[\left(\frac{1}{\mathrm{LIV}}\right)\left(1-e^{-\mathrm{LIV}/\tau_i}\right)-\left(\frac{1}{\mathrm{LAB}}\right)\left(1-e^{-\mathrm{LAB}/\tau_i}\right)\right]}{\left(\frac{1}{\mathrm{LAB}}\right)\left(1-e^{-\mathrm{LAB}/\tau_i}\right)}, \qquad (19)$$

where LAB = LIV $(1 + n\tau_{sat})$.

The second dead-time factor, the preamplifier dead time (τ_{adt}), was determined by placing a hot ^{11}C source on the NaI and comparing the high count rates to that expected by extrapolating the low count rates. The half-life of ^{11}C is sufficiently long to keep the signal-analysis-time correction negligible. The lost counts were least-squares fitted to an exponential $e^{n\tau_{adt}}$, where n is the count rate. The dead time so determined was 3.5 μsec, or about the width of the double-delay line-shaped pulse. However, a best χ^2 fit for the ^{11}C decay was found for τ_{adt} = 4.5 μsec. A compromise of 3.8 μsec was used, which gives a 1% correction at a count rate of 160×10^3 counts/min.

<u>^{4}He Absorption in the Atmosphere</u> Measurements of ^{4}He absorption in the atmosphere are affected by the fragmentation of the Z > 2 cosmic rays and by $^4He \rightarrow {}^3He$ stripping reactions (assuming that the detectors are unable to separate ^{4}He from ^{3}He). We can estimate the effect of the ^{4}He production from the Z > 2 cosmic rays with the transport equation [Eq. (1)]. Neglecting ionization energy loss and reducing the incremental in x to a differential, we are left

with (for He development),

$$\frac{d}{dx}\mathrm{He}(x) + \frac{1}{\Lambda_{He}}\mathrm{He}(x) = \sum_{\substack{i\\(Z>2)}} \frac{N_i(x)}{\Lambda_i} P_{i_{He}}. \qquad (20)$$

The equation for $N_i(x)$ is the same as the above for He, except for leaving off the source on the right-hand side (rhs). This introduces an error of significance only in the L group. $N_i(x)$ can then be written as $N_i(x) = A_i\, e^{-x/\Lambda_i}$, where A_i is the relative abundance to He at the top of the atmosphere. The rhs of Eq. (20) is 15% of the second term on the lhs at x = 0, and diminishes as x increases ($\Lambda_i < \Lambda_{He}$). The He functional form does not differ much from a simple exponential. Setting $\mathrm{He}(x) = e^{-x/\Lambda}$, and averaging the He flux over the first ζ g/cm^2 of the atmosphere [integrating Eq. (20) from x = 0 to x = ζ], we find

$$\frac{\Lambda-\Lambda_{He}}{\Lambda}\left(1-e^{-\zeta/\Lambda}\right) = \sum_{\substack{i\\(Z>2)}} A_i P_{i_{He}}\left(1-e^{-\zeta/\Lambda_i}\right). \qquad (21)$$

Consistent with the approximation needs, we group the source elements into L, M, and H ($Z \geq 10$) groups. Using the fluxes of Von Rosenvinge et al.[5] and Webber and Ormes,[15] the ionization-corrected Λ_{atn} of Webber and Ormes,[15] the $P_{i_{He}}$ in air of Friedlander et al.,[35] and Λ_{He} from Table IV of 44 g/cm^2, we minimize Eq. (21) for Λ, parameterized by ζ, and find

ζ(g/cm^2)	20	50	100	150
Λ(g/cm^3)	50	49	48	48

Equating, in the atmosphere, $\Lambda_{He\ abs}$ to $\Lambda_{He\ atn}$ may introduce an overestimation of $\Lambda_{He\ abs}$ from the spallation of the heavier-than-He cosmic rays of $\approx (9-14)\%$.

The effect on $\Lambda_{He\ abs}$ measurements from $^4He \rightarrow {}^3He$ stripping in the atmosphere can be estimated from the $^4He(n, np)^3H$, $^4He(n, d)^3H$, and $^4He(n, 2n)^3He$ cross sections of $(55 \pm 5)\%$, $(2 \pm 1)\%$, and $(3 \pm 1)\%$ of $\sigma_{^4He, re}^{\ n}$ respectively, measured by Innes[36] at 300 MeV. If we invoke charge symmetry, the first two cross sections should be equal to $\sigma[^4He\,(p, pn)^3He]/\sigma_{^4He, re}^{\ p}$ and $\sigma[^4He(p, d)^3He]/\sigma_{^4He, re}^{\ p}$. Averaging ^3He production over p and n,

$$\frac{\sigma[^4He(n, 2n)^3He] + \sigma[^4He(p, pn)^3He] + \sigma[^4He(p, d)He^3]}{2\sigma_{^4He, re}^{\ p}} = 0.30 \pm 0.03, \qquad (22)$$

and assuming that this ratio holds in the atmosphere for $\sigma[^4He(atm,)^3He]/\sigma_{^4He, re}^{\ p}$, we have $\Lambda_{^4He\ abs} = (1-P_{^4He,\ ^3He})\Lambda_{He\ abs} = (1-0.30 \pm 0.03)\Lambda_{He\ abs} = (0.70 \pm 0.03)_{He\ abs}$. The factor 0.70 ± 0.03 should be taken as a lower bound, as it is expected that the collisions of ^4He with the centers of ^{14}N and ^{16}O will be less effective than with the surfaces of ^{14}N and ^{16}O for single-nucleon knockouts from the ^4He. Taking $\Lambda_{He\ abs} = 44\ g/cm^2$, then $\Lambda_{^4He\ abs}$, considering just stripping reactions, equals $31\ g/cm^2$--a small number in view of geometric calculations (Table IV).

REFERENCES

1. A. G. W. Cameron, in Origin and Distribution of the Elements, edited by L. H. Ahrens (Pergamon Press, New York, 1967).
2. J. Audouze, M. Epherre, and H. Reeves, in High Energy Nuclear Interactions in Astrophysics, edited by B. S. P. Shen (W. A. Benjamin Inc., New York, 1967).
3. J. Radin, Phys. Rev. C, 2, 793 (1970).
4. P. Fontes, C. Perron, J. Lestringuez, F. Yiou, and R. Bernas, Mass-Spectrometric Measurements of Lithium and Beryllium Production Cross Sections in ^{12}C Spallation by High Energy Protons and α Particles (to be published).
5. T. T. von Rosenvinge, J. F. Ormes, and W. R. Webber, Astrophys. Space Sci. 3, 80 (1969); T. T. von Rosenvinge and W. R. Webber, Astrophys. Space Sci. 3, 4 (1969).
6. C. M. Lederer, J. M. Hollander, and I. Perlman, Table of Isotopes 6th ed. (John Wiley and Sons, Inc., New York, 1967).
7. W. S. Gilbert, D. Keefe, J. B. McCaslin, H. W. Patterson, A. R. Smith, L. D. Stephens, K. B. Shaw, G. R. Stevenson, R. H. Thomas, R. D. Fortune, and K. Goebel, Lawrence Radiation Laboratory Report UCRL-17941, 1968 (unpublished).
8. H. Fuch and K. H. Lindenberger, Nucl. Instr. Meth. 7, 219 (1960); J. B. Cumming, A. M. Poskanzer, and J. Hudis, Phys. Rev. Letters 6, 484 (1961).
9. L. Valentin, G. Albouy, J. Cohen, and M. Gusakow, Phys. Letters 7, 163 (1963).
10. V. Parikh, Nucl. Phys. 18, 646 (1960).

11. P. Benioff, Phys. Rev. 119, 316 (1960); P. Benioff, Thesis, Lawrence Radiation Laboratory Report UCRL-8780, 1959 (unpublished).

12. J. B. Cumming, Ann. Rev. Nucl. Sci. 13, (1963).

13. R. Silberberg, private communication, 1969; see also Ref. 2.

14. F. Yiou, C. Seide, and R. Bernas, J. Geophys. Res. 74, 2447 (1969).

15. W. R. Webber and J. F. Ormes, J. Geophys. Res. 72, 5957 (1967).

16. M. M. Shapiro, R. Silberberg, and C. H. Tsao, Source Distribution of Cosmic Ray Abundances, presented at the Midwest Cosmic Ray Conf., Baton Rouge, La., 1969.

17. F. Beck and F. Yiou, Astrophys. Letters 1, 75 (1968).

18. R. Serber, Phys. Rev. 72, 1114 (1947).

19. B. A. Munir, Phil. Mag. (Ser. 8) 1, 355 (1956).

20. G. Alexander and G. Yekutieli, Nuovo Cimento 19, 103 (1961).

21. H. L. Bradt and B. Peters, Phys. Rev. 77, 54 (1950).

22. R. R. Daniel and N. Durgaprasad, Nuovo Cimento Suppl. 23, 82 (1962).

23. T. F. Cleghorn, P. S. Freier, and C. J. Waddington, Can. J. Phys. 46, S572 (1968).

24. C. J. Waddington, Progr. Nucl. Phys. 8 (1963).

25. W. R. Webber and F. B. McDonald, Phys. Rev. 100, 1460 (1955).

26. L. R. Davis, H. M. Caulk, and C. Y. Johnson, Phys. Rev. 101, 800 (1956).

27. F. B. McDonald, Phys. Rev. 104, 1723 (1956).

28. M. S. Kozodaev, M. M. Kulyukin, R. M. Sulyaev, A. I. Filippov, and Y. A. Shcherbakov, Zh. Eksperim. i Teor. Fiz. 38, 708 (1960); Soviet Phys.—JETP 38, 511 (1960).

29. J. A. Lezniak, J. F. Ormes, T. T. Von Rosenvinge, and W. R. Webber, Astrophys. Space Sci. 5, 103 (1969).

30. M. M. Shapiro and R. Silberberg, paper IV, presented at the Eleventh International Conference on Cosmic Rays, Budapest, Hungary, 1969 (to be published).

31. R. Cowsik, Y. Pal, S. N. Tandon, and R. P. Verma, Can. J. Phys. 46, S646 (1968).

32. M. M. Shapiro, R. Silberberg, and C. H. Tsao, The Distribution Function of Cosmic Ray Path Length, paper II, presented at the Eleventh International Conference on Cosmic Rays, Budapest, Hungary, 1969 (to be published).

33. C. E. Fichtel and D. V. Reames, Phys. Rev. 175, 1564 (1968).

34. S. Biswas, Astrophys. Space Sci. 5, 59 (1969).

35. M. W. Friedlander, K. A. Neelakantan, S. Tokunaga, G. R. Stevenson, and C. J. Waddington, Phil. Mag. 8, 1691 (1963).

36. W. H. Innes, Thesis, University of California Radiation Laboratory Report No. UCRL-8040, 1957 (unpublished).

Table I. Decay features of radioisotopes produced (see Ref. 6).

	Isotope				
	^{18}F	^{15}O	^{13}N	^{11}C	^{7}Be
Half-life (min)	109.7	2.05	9.96	20.35	77 180 (53.6 days)
Decay	β^+	β^+	β^+	β^+	478-keV γ
Branching ratio	0.97	1.00	1.00	0.998 taken as 1.00	

Table II. Targets, exposure times, and ratios of cross section to monitor cross section.

Target	Weight (-g)	Length of exposure (sec)	Count rate (counts per min)[a]	Reaction (monitor reaction)	Ratio to monitor (± random error %)	Reaction (monitor reaction)	Ratio to monitor (± random error %)	Reaction (monitor reaction)	Ratio to monitor(± random error %)
Al	0.3968	120	1.15×10^6	$^{27}Al \rightarrow {}^{18}F$ ($^{12}C \rightarrow {}^{11}C$)	0.252 (1.6)				
Al	0.3455	60	1.57×10^6	$^{27}Al \rightarrow {}^{18}F$ ($^{12}C \rightarrow {}^{11}C$)	0.258 (1.6				
Systematic errors in the above ratios					0.0%				
BeO	2.983	6	2.04×10^6	$^{16}O \rightarrow {}^{15}O$ ($^{12}C \rightarrow {}^{11}C$)	0.957 (2.3)	$^{16}O \rightarrow {}^{13}N$ ($^{12}C \rightarrow {}^{11}C$)	0.135 (6.4)	$^{16}O \rightarrow {}^{11}C$ ($^{12}C \rightarrow {}^{11}C$)	0.384 (2.2)
BeO	2.897	4	0.106×10^6	$^{16}O \rightarrow {}^{15}O$ ($^{12}C \rightarrow {}^{11}C$)	0.950 (1.8)	$^{16}O \rightarrow {}^{13}N$ ($^{12}C \rightarrow {}^{11}C$)	0.141 (6.6)	$^{16}O \rightarrow {}^{11}C$ ($^{12}C \rightarrow {}^{11}C$)	0.377 (3.1)
BeO[b]	2.897	4	0.763×10^6	$^{16}O \rightarrow {}^{15}O$ ($^{12}C \rightarrow {}^{11}C$)	0.680 (1.8)	$^{16}O \rightarrow {}^{13}N$ ($^{12}C \rightarrow {}^{11}C$)	0.125 (5.8)	$^{16}O \rightarrow {}^{11}C$ ($^{12}C \rightarrow {}^{11}C$)	0.370 (2.0)
Systematic errors in the above ratios					1.0%		1.0%		1.0%
$(CH)_n$	1.907	60	20.5	$^{12}C \rightarrow {}^{7}Be$ ($^{12}C \rightarrow {}^{11}C$)	0.397 (6.3)	$^{12}C \rightarrow {}^{7}Be$ ($^{27}Al \rightarrow {}^{18}F$)	1.58 (6.3)		
$(CH)_n$	1.705	120	35.8	$^{12}C \rightarrow {}^{7}Be$ ($^{12}C \rightarrow {}^{11}C$)	0.403 (7.5)	$^{12}C \rightarrow {}^{7}Be$ ($^{12}Al \rightarrow {}^{18}F$)	1.54 (3.7)		
$(CH)_n$	1.843	600	197	$^{12}C \rightarrow {}^{7}Be$ ($^{12}C \rightarrow {}^{11}C$)	0.413 (1.8)	$^{12}C \rightarrow {}^{7}Be$ ($^{27}Al \rightarrow {}^{18}F$)	1.59 (1.8)		
$(CH)_n$[c]	1.975	300	134	$^{12}C \rightarrow {}^{7}Be$ ($^{12}C \rightarrow {}^{11}C$)	0.354	$^{12}C \rightarrow {}^{7}Be$ ($^{27}Al \rightarrow {}^{18}F$)	1.60		
$(CH)_n$	1.950	600	200	$^{12}C \rightarrow {}^{7}Be$ ($^{12}C \rightarrow {}^{11}C$)	0.413 (2.5)	$^{12}C \rightarrow {}^{7}Be$ ($^{27}Al \rightarrow {}^{18}F$)	1.62 (2.5)		
$(CH)_n$	1.916	600	189	$^{12}C \rightarrow {}^{7}Be$ ($^{12}C \rightarrow {}^{11}C$)	0.416 (2.5)	$^{12}C \rightarrow {}^{7}Be$ ($^{27}Al \rightarrow {}^{18}F$)	1.57 (2.5)		
Systematic errors in the above ratios					2.0%		2.0%		
BeO	2.991	600	245	$BeO \rightarrow {}^{7}Be$ ($^{12}C \rightarrow {}^{11}C$)	0.631 (2.4)	$BeO \rightarrow {}^{7}Be$ ($^{27}Al \rightarrow {}^{18}F$)	2.61 (2.5)	$BeO \rightarrow {}^{7}Be$ ($^{12}C \rightarrow {}^{7}Be$)	1.528 (3.1)
BeO	10.82	120	181	$BeO \rightarrow {}^{7}Be$ ($^{12}C \rightarrow {}^{11}C$)	0.623 (7.3)	$BeO \rightarrow {}^{7}Be$ ($^{27}Al \rightarrow {}^{18}F$)	2.48 (3.2)	$BeO \rightarrow {}^{7}Be$ ($^{12}C \rightarrow {}^{7}Be$)	1.538 (3.8)
Systematic errors in the above ratios					2.4%		2.4%		1.0%
Be	1.474	600	133	$^{9}Be \rightarrow {}^{7}Be$ ($^{12}C \rightarrow {}^{11}C$)	0.263 (2.4)	$^{9}Be \rightarrow {}^{7}Be$ ($^{27}Al \rightarrow {}^{18}F$	1.016 (2.4)	$^{9}Be \rightarrow {}^{7}Be$ ($^{12}C \rightarrow {}^{7}Be$	0.628 (3.0)
Be	1.474	600	144[d]	$^{9}Be \rightarrow {}^{7}Be$ ($^{12}C \rightarrow {}^{11}C$)	0.261 (3.2)	$^{9}Be \rightarrow {}^{7}Be$ ($^{27}Al \rightarrow {}^{18}F$)	0.992 (3.2)	$^{9}Be \rightarrow {}^{7}Be$ ($^{12}C \rightarrow {}^{7}Be$)	0.628 (3.3)
Systematic errors in the above ratios					2.2%		2.2%		0.0%

[a] Count rate above background, at end of exposure, of isotopes in the adjacent column.
[b] Run discarded because of large deviation.
[c] Run discarded because of large χ^2 in the fit.
[d] Count rate above residual count rate from previous exposure.

Table III. α-Particle and p cross sections,[a] and Σ_p^α at $E_p = E_\alpha$ (230 MeV/N) and at $E_p = E_{\alpha T}$ (920 MeV).

Reaction	ΔA	σ_α (mb) 920 MeV	σ_p (mb) 230 MeV	Σ_p^α $E_p = E_\alpha$	σ_p (mb) 920 MeV	Σ_p^α $E_p = E_{\alpha T}$
$^9Be \rightarrow {}^7Be$	2	12.7 ±0.6	11.4±0.5	1.11±0.1	13.8±1	0.92±0.1
$^{12}C \rightarrow {}^{11}C$	1	49.4 ±1.8	38±2	1.30±0.08	28±1.4	1.76±0.11
$^{12}C \rightarrow {}^7Be$	5	20.2 ±1.1	9.9±1	2.04±0.24	10.0±1	2.02±0.24
$^{16}O \rightarrow {}^{15}O$	1	47.1 ±2.3	34±4	1.39±0.17	29±3	1.62±0.18
$^{16}O \rightarrow {}^{13}N$	3	6.82±0.5	5.0±1.5	1.36±0.42	5.0±2	1.36±0.54
$^{16}O \rightarrow {}^{11}C$	5	18.7 ±0.9	10±2	1.87±0.4	10±1.5	1.87±0.30
$^{16}O \rightarrow {}^7Be$	9	18.7 ±1.4	5.9±1.5	3.2 ±0.8	{8.0±1.5[b] / 9.0±1.5	{2.34±0.47 / 2.07±0.37[b]
$^{27}Al \rightarrow {}^{18}F$	9	12.6 ±0.5	6.0±0.4	2.08±0.15	8.05±0.5	1.57±0.13

[a] The α-Particle cross sections are from this work except for $\sigma[^{12}C(\alpha, x)^{11}C]$ from Ref. 3. The $^{16}O + p$ cross sections are from Refs. 2 and 13. The $^{12}C + p$ and $^{27}Al + p$ cross sections are from Ref. 12.

[b] At 2 GeV.

Table IV. Intercomparison of different models for interaction mean free paths in emulsion and air.

	Adopted experimental value	Independent-particle optical potential[a]	Three overlap models $\sigma_{i,re}^\alpha = \pi(r_0 A_\alpha^{1/3} + r_0 A_i^{1/3} - \Delta r)^2$		
r_0 (F)			1.45[b]	1.17[c]	1.20[d]
Δr (F)			1.70[b]	0.0[c]	0.50[d]
Λ_{emul}(g/cm^2)[e]	77[f]	75.6±0.3[g]	77.6	69.9	77.9
Λ_{air}(g/cm^2)	44[f]	42.5	47.0	36.2	42.9
$\sigma_{^{16}O,\,re}^\alpha$(mb)		600±10[h]	569	725	616

[a] With a free nucleon-nucleon cross section of 40 mb. See Ref. 18.
[b] See Ref. 19.
[c] See Ref. 20.
[d] See Ref. 21.
[e] With $\sigma_{\alpha,\,re}^p$ = 125 mb. See Ref. 26.
[f] See text.
[g] Value read from a graph and adjusted with $\sigma_{\alpha,\,re}^p$ = 125 mb.
[h] Value read from a graph.

Table V. Quantity of interstellar gas traversed and elemental ratios to carbon, parameterized by the He/H+He ratio of the interstellar gas, at L/M = 0.25.

Value of He/H+He used for			Amount of gas traversed				Elemental ratios to carbon[b]				
Λ_i	P_{ij}	dE/dx	g/cm^2	%[a]	atoms/cm^{2}N$_0$	%[a]	Li	Be	B	N	O
experimental observations[c]							0.15±0.01	0.12±0.02	0.27±0.02	0.26±0.02	0.89±0.02
0.0	0.0	0.0	4.61	---	4.61	---	0.15	0.083	0.29	0.26	0.83
0.1	0.1	0.1	5.49	+19.2	4.23	-8.16	+1.47	+1.00	-0.62	-0.53	+0.77
0.2	0.2	0.2	6.24	+35.5	3.91	-15.1	+2.81	+1.85	-1.14	-0.95	+1.43
0.2	0.0	0.0	5.67	+23.0			+0.40	+0.65	+1.31	+0.27	+2.30
0.0	0.2	0.0	5.04	+ 9.49			+2.21	+0.76	-2.90	-2.01	-1.50
0.0	0.0	0.2	4.62	+ 0.33			+0.13	+0.27	+0.17	+0.42	+0.35
Sum of the partial He/H+He = 0.2				+32.8			+2.74	+1.68	-1.42	-1.32	+1.15
0.1	0.0	0.0	5.18	+12.4			+0.22	+0.35	+0.71	+0.15	+1.24
0.0	0.1	0.0	4.84	+ 5.13			+1.20	+0.41	-1.57	-1.09	-0.81
0.0	0.0	0.1	4.62	+ 0.19			+0.07	+0.15	+0.09	+0.23	+0.19
Sum of the partial He/H+He = 0.1				+17.7			+1.49	+0.91	-0.77	-0.71	+0.62

Uncertainties on the signed (+ or -) fractional-elemental ratio changes are ≤ 5%.

[a]Percent difference from the case of interstellar gas consisting of 100% hydrogen (row 2).

[b]Except for rows 1 and 2, the same as in footnote a.

[c]See Refs. 5, 27, 28, 16.

FIGURE CAPTIONS

Fig. 1. Target arrangements. α-Particle beam incident from the left. Target subsets (1, 2, and 3) consist of 2 guard foils and a central, counted disk (see text). Set a: for ^{27}Al → ^{18}F and for ^{12}C → ^{7}Be; 1, Al; 2, $(CH)_n$. For ^{16}O → (^{15}O, ^{13}N, ^{11}C); 1, $(CH)_n$; 2, BeO. Set b: 1, $(CH)_n$; 2, Al; for ^{12}C → ^{7}Be and BeO → ^{7}Be; 3, BeO; for ^{12}C → ^{7}Be and ^{9}Be → ^{7}Be; 3, Be.

Fig. 2. Σ_p^α at $E_p = E_{\alpha T}$(920 MeV). □, ^{27}Al target; O, ^{16}O target; χ, ^{12}C target; ∇, ^{9}Be target. Curves (a) and (b) are the linear fits of $\Sigma_p^\alpha(\Delta A)$ to the ^{12}C and ^{16}O target cross sections, with the values for $\sigma[^{16}O(p,x)\,^{7}Be]$ at 2 GeV (a) or at 920 MeV (b).

Fig. 3. ^{7}Be excitation functions for p + ^{9}Be and p + ^{16}O (see text). The error bar on the ^{16}O curve is constant for the length of the curve.

Fig. 4. Percent change in elemental abundance ratios (to carbon) for He/H+He = 0.1 relative to He/H+He = 0.0, at L/M = 0.25. Column (parameter of interaction for which He/H+He = 0.1): 1 (Λ); 2 (P_{ij}); 3 (dE/dx); 4 \\\\ is the sum of columns 1-3, //// is He/H+He = 0.1). Uncertainties are ≤ 5%.

Fig. 5. The quantity [(% change in elemental abundance) - ⟨ % change in elemental abundance in L or M group⟩] for He/H+He = 0.1 relative to He/H+He = 0.0, at L/M = 0.25. Column (parameter of interaction for which He/H+He = 0.1): 1 (Λ); 2 (P_{ij}); 3 (dE/dx); 4 (//// is the sum of columns 1-3, \\\\ is He/H+He = 0.1). Uncertainties are less than or equal to the uncertainty shown.

Fig. 6. Fractional change in the mass $[x(g/cm^2)]$ of interstellar space traversed to produce $L/M = 0.25$, as a function of $R \equiv He/H+He$ relative to $He/H+He = 0.0$. The curve is the fit to $1.94\ R\ \exp(-0.56\ R)$ which differs from the calculated fractional change by $< 3\%$ for all R.

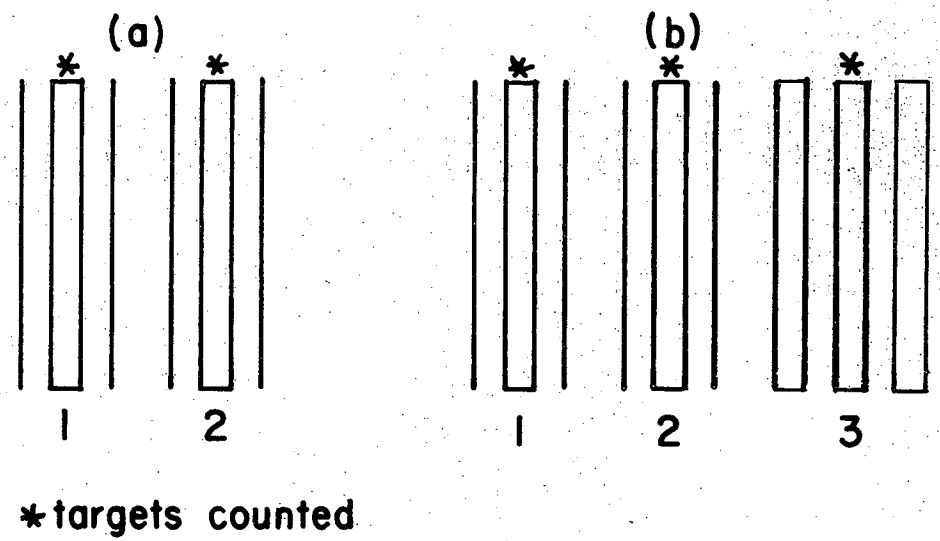

XBL 712-316

Fig. 1

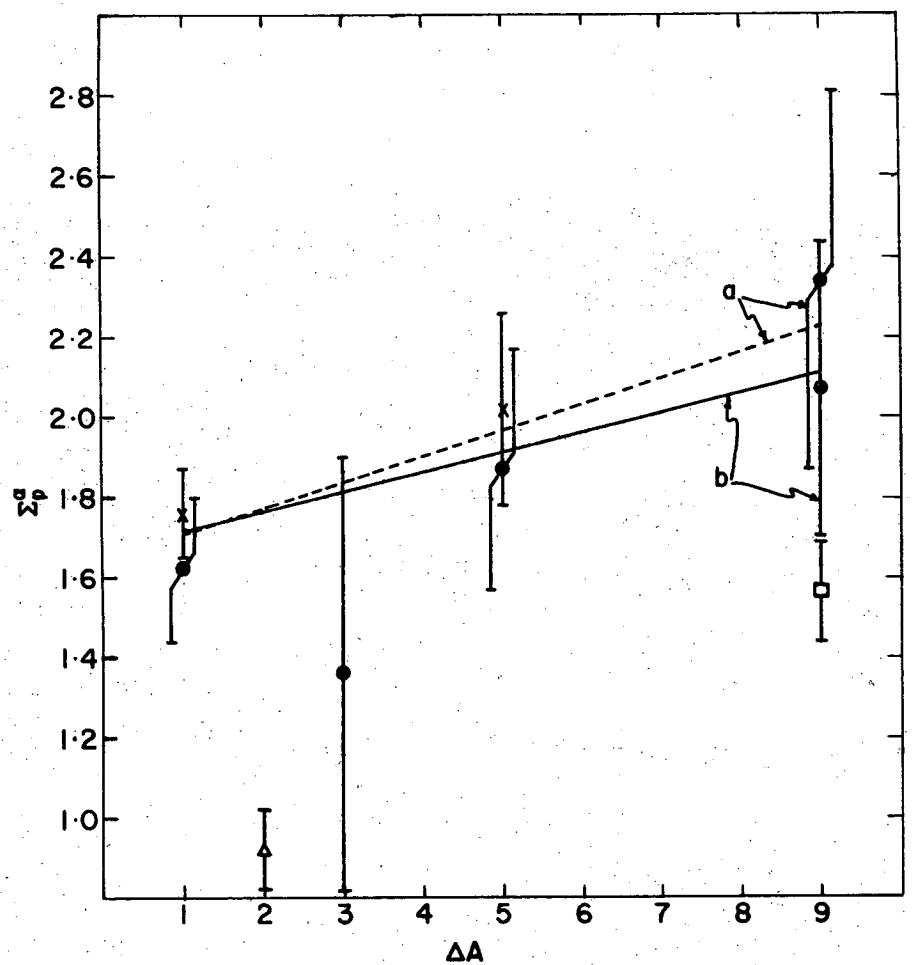

XBL 712-315

Fig. 2

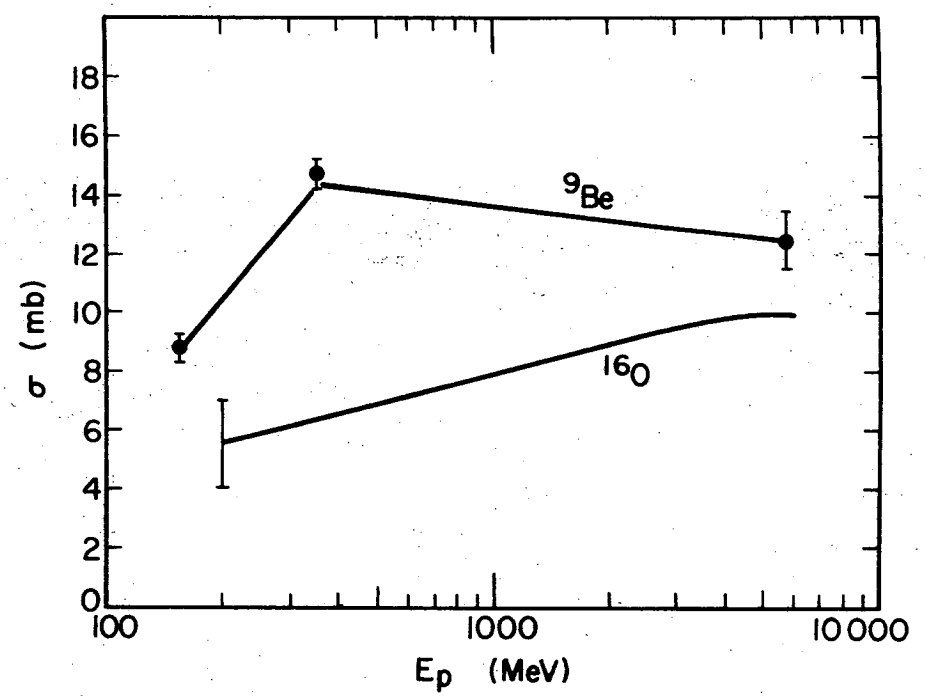

XBL 712-314

Fig. 3

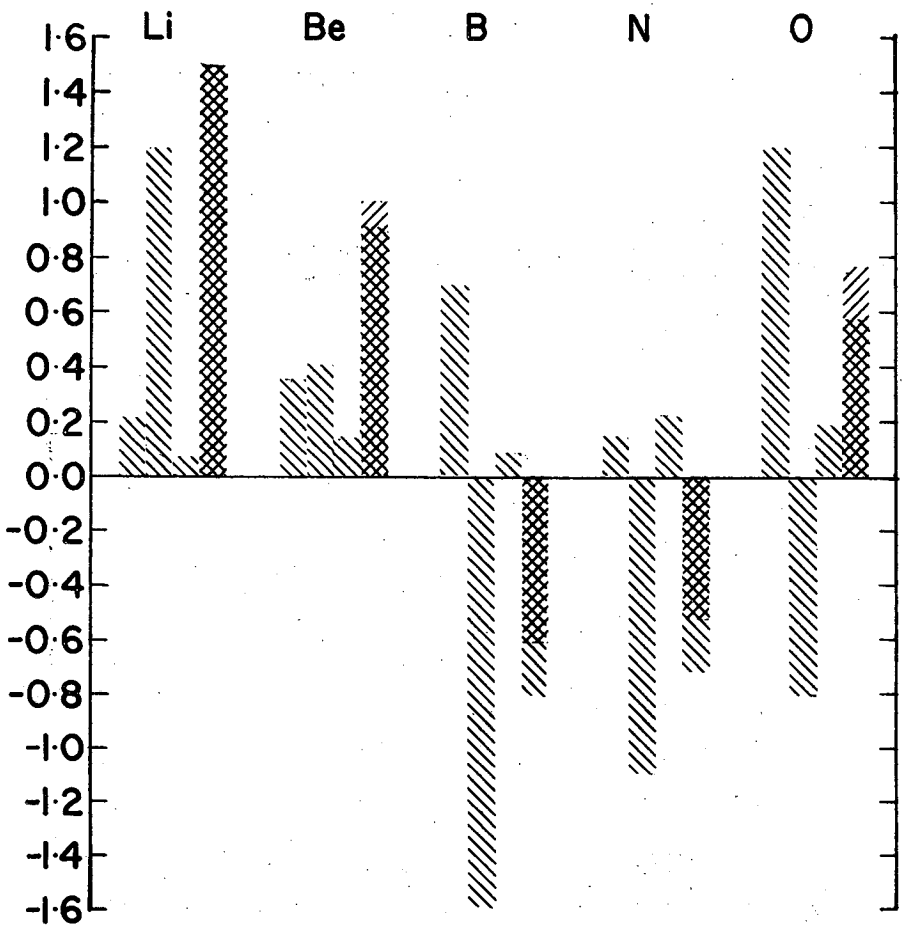

XBL 712-313

Fig. 4

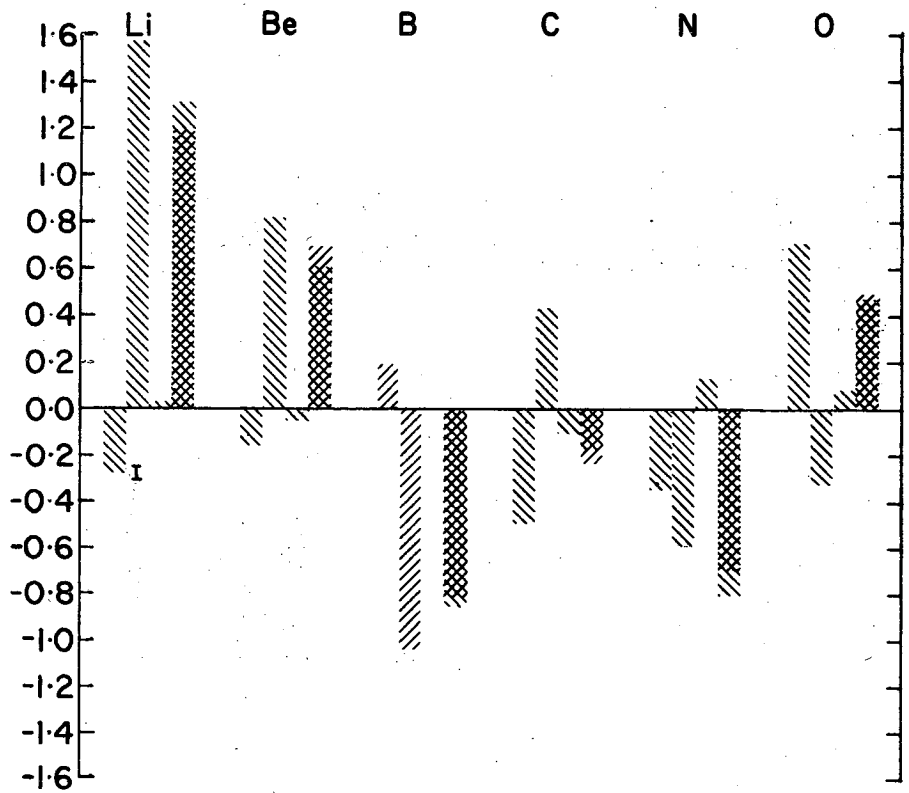

XBL 712-312

Fig. 5

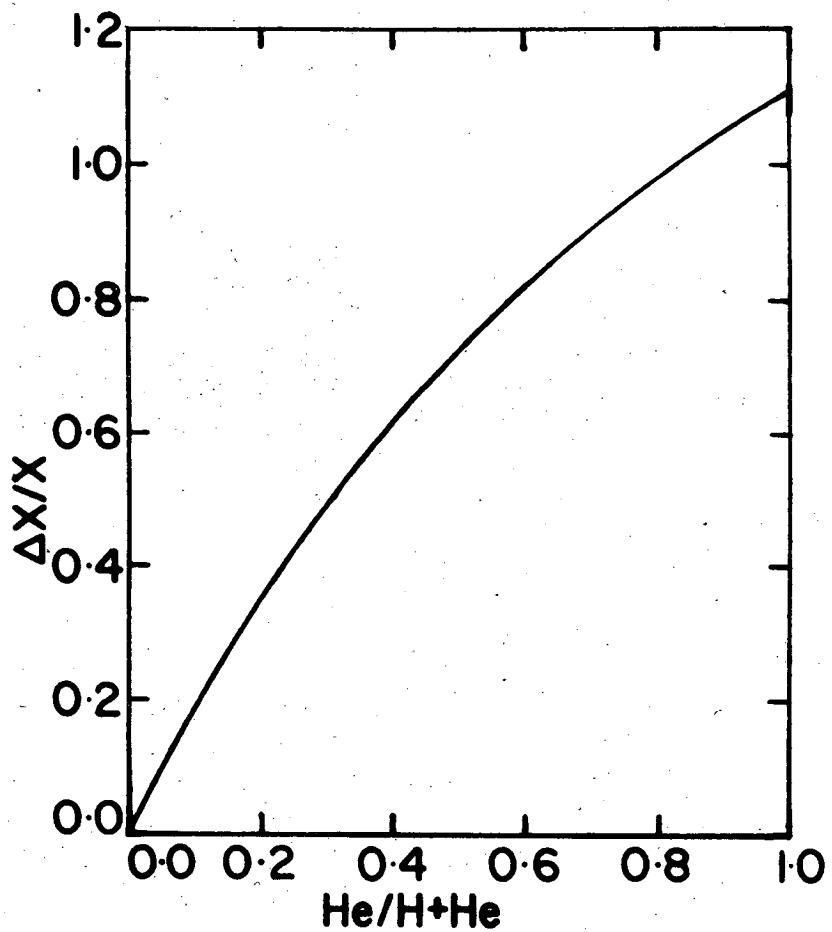

XBL 712-311

Fig. 6

LEGAL NOTICE

This report was prepared as an account of work sponsored by the United States Government. Neither the United States nor the United States Atomic Energy Commission, nor any of their employees, nor any of their contractors, subcontractors, or their employees, makes any warranty, express or implied, or assumes any legal liability or responsibility for the accuracy, completeness or usefulness of any information, apparatus, product or process disclosed, or represents that its use would not infringe privately owned rights.

TECHNICAL INFORMATION DIVISION
LAWRENCE RADIATION LABORATORY
UNIVERSITY OF CALIFORNIA
BERKELEY, CALIFORNIA 94720